



**QUEEN'S
UNIVERSITY
BELFAST**

Broadband Parallel-Circuit Class-E Amplifier with Second Harmonic Control Circuit

Akram Sheikhi, Thian, M., & Mehrnosh Vafaee (2019). Broadband Parallel-Circuit Class-E Amplifier with Second Harmonic Control Circuit. *IEEE Transactions on Circuits and Systems II: Express Briefs*, 66(6), 928-932. <https://doi.org/10.1109/TCSII.2018.2874983>

Published in:
IEEE Transactions on Circuits and Systems II: Express Briefs

Document Version:
Peer reviewed version

Queen's University Belfast - Research Portal:
[Link to publication record in Queen's University Belfast Research Portal](#)

Publisher rights
© 2018 IEEE.

This work is made available online in accordance with the publisher's policies. Please refer to any applicable terms of use of the publisher.

General rights

Copyright for the publications made accessible via the Queen's University Belfast Research Portal is retained by the author(s) and / or other copyright owners and it is a condition of accessing these publications that users recognise and abide by the legal requirements associated with these rights.

Take down policy

The Research Portal is Queen's institutional repository that provides access to Queen's research output. Every effort has been made to ensure that content in the Research Portal does not infringe any person's rights, or applicable UK laws. If you discover content in the Research Portal that you believe breaches copyright or violates any law, please contact openaccess@qub.ac.uk.

Broadband Parallel-Circuit Class-E Amplifier with Second Harmonic Control Circuit

Akram Sheikhi, Mury Thian, and Mehrnosh Vafaei

Abstract— This paper presents the analysis and coherent design method of a high-efficiency broadband parallel-circuit Class-E power amplifier with second harmonic control circuit. The PA's broadband characteristic is achieved through analysis of the load network using double reactance compensation technique. Using a high power LDMOS transistor and operated from a 35 V supply voltage, the practical PA exhibits 41.5-44.1 dBm output power and 79-82.2% drain efficiency over 115-155 MHz frequency range. The measurement results show good agreements with the simulation results and theory.

Index Terms—Amplifier, broadband, Class-E, harmonic trap, high efficiency, parallel-circuit, reactance compensation.

I. INTRODUCTION

SWITCHED-mode and harmonically tuned power amplifiers (PAs) have been widely used due to their simple structure and high efficiency characteristics, [1]-[8]. The Class-E with shunt capacitance topology reported in [6] and analyzed in [7] employs an ideal RF choke to provide an infinite impedance at both fundamental and harmonic frequencies, which renders its implementation challenging. In contrast, the parallel circuit Class-E topology described in [8] uses a finite dc-feed inductance, thereby offering compact size, low cost, and improved efficiency due to lower equivalent series resistance (ESR). Furthermore, when compared to the Class-E with shunt capacitance, the parallel-circuit Class-E PA offers higher maximum operating frequency and higher load resistance leading to a lower loss due to reduced impedance transformation ratio.

Wideband power amplifiers are required for deployment in modern wireless communication systems to enable high data rate transmission. Many techniques have been proposed to increase the inherent bandwidth of the Class-E PA, [9]-[15]. A differential wideband load transformation network was introduced in [9]. Using a combination of a finite dc-feed inductance and low-pass filters result in wideband Class-E amplifiers [10]. The work in [11] proposed a broadband lumped-element impedance matching technique that leads to high output power and high efficiency. However, this technique requires an additional network to transform 50Ω to the Class-E's optimum load resistance. Wide bandwidth can also be achieved using reactance compensation techniques [12]-[15].

The basic circuits of the classical Class-E with shunt capacitance and the parallel-circuit Class-E power amplifier are

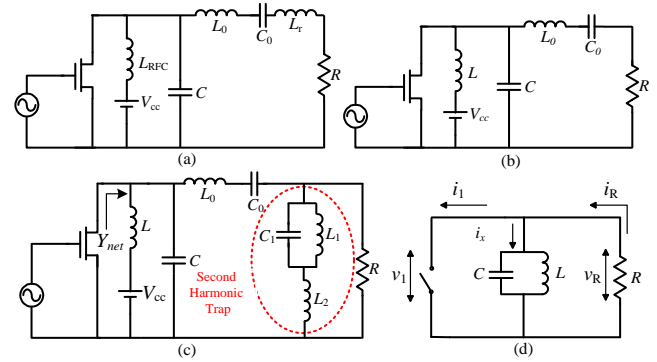


Fig. 1. Basic circuit of (a) the Class-E with shunt capacitance, (b) the parallel-circuit Class-E, (c) the proposed parallel-circuit Class-E with second harmonic trap, and (d) its equivalent circuit at the fundamental frequency.

shown in Fig. 1(a) and Fig. 1(b), respectively. In the Class-E mode, the current and voltage waveforms of the active device are shaped such that their overlap in time domain is minimal, thus minimizing power dissipation within the active device and maximizing the DC-to-RF efficiency. This is achieved through applying zero voltage switching (ZVS) and zero voltage derivative switching (ZVDS) conditions.

In this paper, a new variant of the parallel-circuit Class-E PA is proposed, Fig. 1(c). The load network of the proposed circuit is comprised of a parallel-tuned resonator $L-C$ where L doubles as a finite dc-feed inductance, a series-tuned resonator L_0-C_0 where C_0 doubles as a finite dc-blocking capacitance, a second-harmonic trap composed of a parallel resonator L_1-C_1 in series with an inductor L_2 , and a resistor R . Compared with the parallel-circuit Class E, our circuit incorporates a second harmonic trap that is realized using a mixed parallel-series resonant circuit, i.e. $L_1-C_1-L_2$. This load network is analyzed in the frequency domain using double reactance compensation technique to maximize the bandwidth of the proposed PA. The second harmonic trap circuit presents a low impedance to the ground to the second harmonic component whereas the series resonator L_0-C_0 presents a high impedance to other higher harmonic components (3^{rd} , 4^{th} , etc.) and prevents them from appearing at the output, thereby reducing the total harmonic distortion (THD) of the PA.

II. CIRCUIT ANALYSIS

The circuit schematic of the proposed PA and its equivalent circuit at the fundamental frequency (f_0) are shown in Figs. 1(c)-(d). Both the series resonator L_0-C_0 and parallel resonator L_1-C_1

Manuscript submitted March 10, 2018. Akram Sheikhi is the Faculty Member of the Electrical Engineering Department, Lorestan University, Khorramabad, Iran (e-mail: akram.sheikhi2008@gmail.com). Mury Thian is

with the Queen's University of Belfast, ECIT Institute, United Kingdom (e-mail: m.thian@qub.ac.uk). And Mehrnosh Vafaei is with Lorestan University (e-mail: mhrnsh.vafaei@gmail.com @gmail.com).

are tuned at f_0 , thus provide a short and open circuit, respectively. At $2f_0$, the resonator L_1 - C_1 behaves like a capacitance, which is resonated with L_2 to provide a short circuit. The circuit is analyzed using the following assumptions:

- The switch is ON for $0 < \omega t < \pi$ and OFF for $\pi < \omega t \leq 2\pi$ interval, implying a 50% duty ratio.
- The output current is sinusoidal with the initial phase shift ϕ .
- To simplify the analysis with an aim to arrive at some meaningful design insights, the transistor is modelled as an ideal switch in parallel with a shunt capacitor C . Large transistors typically employed in low-frequency high-power applications such as ours have low (negligible) R_{ON} and considerably high C_{OFF} values. Therefore, in our analysis, only C_{OFF} is taken into account i.e. modelled as a linear capacitance C . In [16], it was shown that it is sufficient to approximate the nonlinear output capacitance of the transistor with a linear capacitance.

In the analysis of the idealized parallel-circuit Class-E PA [8], two optimum conditions, i.e., ZVS given in (1) and ZVDS given in (2) are applied. When the transistor is turned ON, current flows through the switch but with no voltage produced across it. When the transistor is turned OFF, no current flows through the switch, and the switch voltage is equal to the voltage across the charged shunt capacitor C . Since the switch voltage and current do not overlap, no power is dissipated within the switch, resulting in a theoretical 100% DC-to-RF efficiency. Two quadrature fundamental-frequency currents i_R and i_X in Fig. 1(d) can be determined using Fourier integrals, and represented as the phase angle of the load network seen from the device drain at f_0 , (3).

$$v(\omega t)|_{\omega t = 2\pi} = 0 \quad (1)$$

$$\frac{dv(\omega t)}{d\omega t}|_{\omega t = 2\pi} = 0 \quad (2)$$

$$\tan \phi = \frac{R}{\omega L} - \omega RC \quad (3)$$

The impedances of the series resonator L_0 - C_0 and the parallel resonator L_1 - C_1 , denoted here as Z_0 and Z_1 respectively, can be expressed as

$$Z_0 = j\omega L_0 + \frac{1}{j\omega C_0} = j\omega' L_0 \quad (4)$$

$$Z_1 = \frac{1}{j(\omega C_1 - \frac{1}{\omega L_1})} = \frac{1}{j\omega' C_1} \quad (5)$$

where

$$\omega' = \frac{\omega^2 - \omega_0^2}{\omega} \quad (6)$$

$$\omega_0^2 = \frac{1}{L_0 C_0} = \frac{1}{L_1 C_1} \quad (7)$$

The admittance of the load network, Y_{net} , can be expressed as

$$Y_{net} = \frac{1}{j\omega L} + j\omega C + \frac{1}{Z_A} \quad (8)$$

where

$$Z_A = Z_0 + \frac{1}{\frac{1}{R} + \frac{1}{Z_2}} \quad (9)$$

$$Z_2 = j\omega L_2 + Z_1 = j\omega L_2 + \frac{1}{j\omega' C_1} \quad (10)$$

Substitutions of (4) and (10) into (9) result in

$$Z_A = j\omega' L_0 + \frac{R(\omega\omega' L_2 C_1 - 1)}{(\omega\omega' L_2 C_1 - 1) - j\omega' R C_1} \quad (11)$$

$$\text{Im}\left(\frac{1}{Z_A}\right) = \frac{-(\omega' R^2 C_1 p + m q)}{R^2 p^2 + q^2} \quad (12)$$

where

$$p = (\omega')^2 L_0 C_1 + m \quad (13a)$$

$$q = \omega' L_0 m \quad (13b)$$

$$m = \omega\omega' L_2 C_1 - 1 \quad (13c)$$

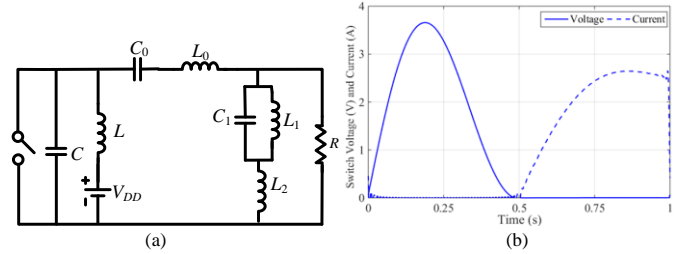


Fig. 2. (a) Simulation setup, (b) ideal switch voltage and current waveforms.

The double reactance compensation technique is applied by setting the first and third derivatives of B with respect to ω to zero as follows:

$$\frac{dB}{d\omega}|_{\omega = \omega_0} = \frac{d^3 B}{d\omega^3}|_{\omega = \omega_0} = 0 \quad (14)$$

where B is the imaginary part of Y_{net} given in (8). This results in a system of two equations, (15)-(16).

$$C + \frac{1}{\omega_0^2 L} - \frac{2L_0 - 2C_1 R^2}{R^2} = 0 \quad (15)$$

$$\frac{6}{\omega_0^4 L} + \frac{6}{\omega_0^2} \left(C_1 - \frac{L_0}{R^2} \right) - \frac{144C_1 L_0^2 + 16C_1 L_0 L_2}{R^2} + 48C_1^2 (\omega_0^2 L_2^2 C_1 + L_0) + \frac{48L_0^3}{R^4} = 0 \quad (16)$$

At f_0 , the inductor L_1 resonates with C_1 , resulting in an open circuit. At $2f_0$, the parallel resonator L_1 - C_1 behaves like a capacitance C_X (17), and resonates with L_2 , thereby presenting a short circuit (18).

$$C_X = \frac{3}{4\omega_0^2 L_1} \quad (17)$$

$$L_2 = \frac{1}{4\omega_0^2 C_X} \quad (18)$$

Substituting (17) into (18) yields

$$L_2 = L_1/3 \quad (19)$$

For specified DC supply voltage V_{DD} (in V), output power P_{out} (in W), and operating frequency ω_0 (in rad/s), the optimum values of the parallel inductance L , capacitance C , and load resistance R can be determined using (20)-(22) as derived in [8]:

$$L = 0.732 \frac{R}{\omega_0} \quad (20)$$

$$C = \frac{0.685}{\omega_0 R} \quad (21)$$

$$R = 1.365 \frac{(V_{DD} - V_{sat})^2}{P_{out}} \quad (22)$$

where V_{sat} is the saturation voltage of the switching device. The phase angle of the load network given in (3) can be determined using (20)-(22), yielding $\phi = 34.24^\circ$. Substitutions of (7), (19) and (20)-(21) into (15)-(16) result in

$$\frac{0.685}{\omega_0 R} + \frac{1}{0.732\omega_0 R} - \frac{2L_0 - 2C_1 R^2}{R^2} = 0 \quad (23)$$

$$\frac{1}{0.122\omega_0^3 R} + 48L_0 \left(\frac{L_0^2}{R^4} + C_1^2 - \frac{3L_0 C_1}{R^2} \right) = \frac{34}{3\omega_0^2} \left(\frac{L_0}{R^2} - C_1 \right) \quad (24)$$

The values of L_0 and C_1 are determined by solving (23)-(24) simultaneously. The values of C_0 , L_1 and L_2 are then calculated using (7) and (19).

III. DESIGN PROCEDURES AND SIMULATIONS

In order to validate the analysis in Section II, we simulated the PA circuit in Fig. 1(c) using an ideal switch model and ideal passive components. The simulation setup with normalized frequency, DC supply voltage and output power is shown in Fig. 2(a). The switch current and voltage waveforms are shown in Fig. 2(b), from which it can be observed that the ZVS and ZVDS conditions are satisfied, and there is no overlap between the switch voltage and current waveforms, leading to a high efficiency close to 100%. The effect of variation in C on the PA efficiency is shown in Fig. 3(a). It can be observed that the efficiency decreases to 80% as C is increased to $1.9 \times$ its theoretical value in (21). Fig. 3(b) shows that when the PA is operated in a suboptimum mode, the ZVS condition is preserved, not affected by the S values ($S=dv_s/d\theta$). Fig. 3(c) shows the effect that the duty ratio has on the switch voltage and current waveforms, from which it can be observed that as the duty ratio is increased, the peak switch voltage increases and the peak switch current decreases.

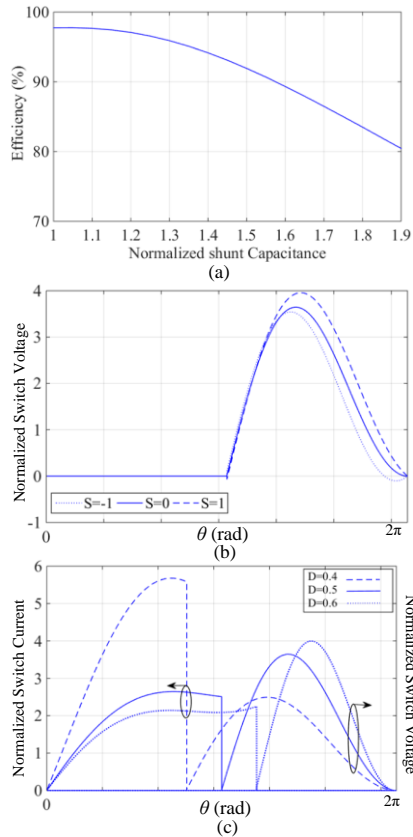


Fig. 3. (a) PA efficiency versus normalized shunt capacitance, (b) normalized switch voltage waveforms at suboptimum and optimum operations, and (c) normalized switch voltage and current waveforms at different duty ratio values.

The complete circuit schematic of the PA including the input matching network and gate biasing circuit is depicted in Fig. 4(a). The transistor used in our design is a high-ruggedness n-

channel enhancement-mode lateral MOSFET (LDMOS) MRFE6VS25N from NXP Semiconductors with a drain-source breakdown voltage of 142 V and peak envelope power of 25 W [17]. Using a 35 V DC supply voltage, the PA was designed to deliver 30 W into a 50Ω load across a 115-155 MHz frequency range.

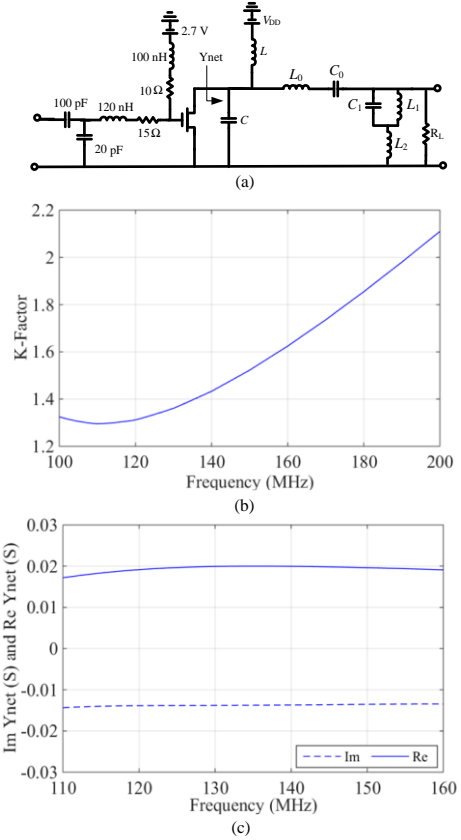


Fig. 4. (a) Complete circuit schematic of the proposed PA, (b) stability factor, (c) real and imaginary parts of the load network's admittance.

Parameters	L	C	L_0	C_0	L_1	C_1	L_2
Theoretical	42.8	16.2	97	14.3	90.8	15.3	30.2
Optimized	47	10	100	14	93	16	31

The theoretical and optimized values of the PA's load network parameters are shown in Table I (all inductors are in nH and capacitors are in pF). The difference between the theoretical and optimized values of the shunt capacitor C is mainly due to the transistor's output capacitance, i.e. $C_{DS} = C_{oss} - C_{rss}$ where C_{oss} and C_{rss} are the output and reverse transfer capacitance of power MOSFET MRFE6VS25NR, respectively. An L-type input matching network, comprised of a series inductor 120 nH and a shunt capacitor 20 pF, is employed to match the input impedance of the MOSFET to the 50Ω source impedance. The ESR of the 120 nH inductor, i.e. 15Ω , helps improve the stability of the PA, resulting in stability factor (K) larger than 1 and stability measure ($B1$) larger than 0. The stability factor of the PA is shown in Fig. 4(b). The real and imaginary parts of the load network's admittance, i.e. $\text{Re}(Y_{net})$ and $\text{Im}(Y_{net})$, are plotted versus frequency in Fig. 4(c), showing the effectiveness of the proposed load network to provide a

constant conductance and susceptance over a wide frequency range.

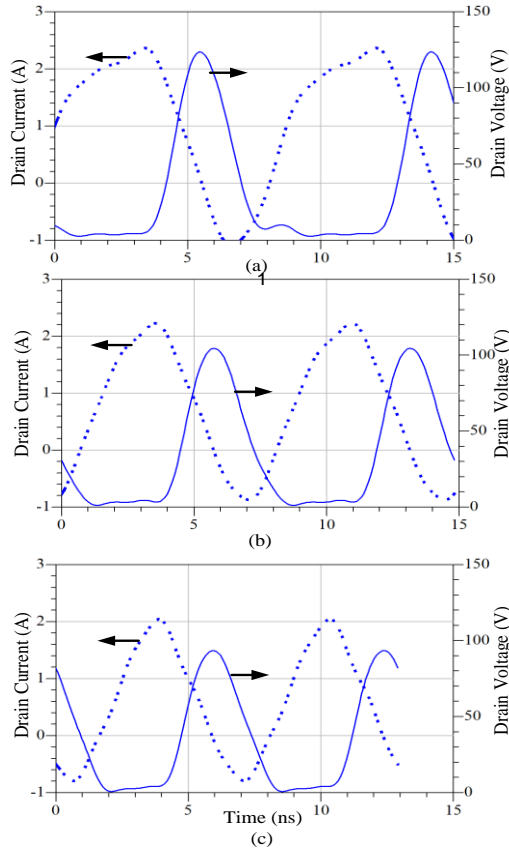


Fig. 5. Simulated drain voltage and current waveforms for $f_0 =$ (a) 115 MHz, (b) 135 MHz, and (c) 155 MHz.

Illustrated in Fig. 5 are the simulated drain voltage and current waveforms for $f_0 = 115$ MHz, 135 MHz, and 155 MHz, from which it can be observed that they resemble the standard Class-E mode waveforms. In particular, the peak drain voltage of the 115 MHz case, i.e. 123 V, is in a good agreement with that of the parallel-circuit Class-E where $V_{\max} = 3.647V_{DD}$. When simulated using the actual transistor model, an overlap between the switch voltage and current waveforms is inevitable due to nonidealities, packaging parasitics, etc., leading to a degradation in efficiency. To minimize this effect, a circuit optimization was performed using the built-in optimizer in ADS with a chief goal to maximize the efficiency while keeping the output power close to the specified value of 25 W. Fig. 6(a) shows that the PA load network presents a relatively constant impedance of $50\ \Omega$ and a phase angle of around 34° over the frequency range of interest. The simulated 2nd and 3rd harmonic suppression levels are depicted in Fig. 6(b). The proposed amplifier exhibits excellent 2nd and 3rd harmonic suppression of better than 30 dBc from 125 to 160 MHz. The 3rd harmonic suppression is achieved since the series resonator L_0 - C_0 provides a high impedance (around $220\ \Omega$) at $3f_0$. The simulated drain efficiency (DE), power added efficiency (PAE), and output power are plotted versus frequency in Fig. 7(a). The proposed PA with second harmonic control circuit and double reactance compensation technique is capable of providing maximum DE of 85%, PAE of 83.6%, and an output power of

44.3 dBm over the 115-155 MHz frequency range. The power gain compresses at 15 dBm input power and efficiency reaches its maximum value at 26 dBm input power. Shown in Fig. 7(b) are the DE and power gain versus output power, wherein the maximum DE is obtained at 44.3 dBm output power.

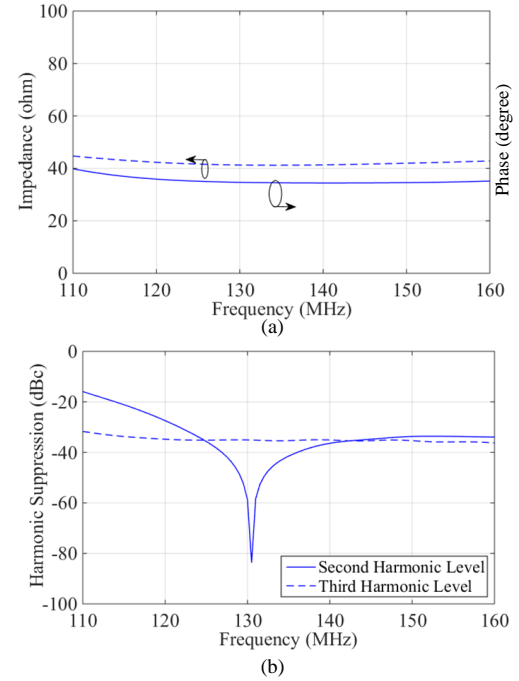


Fig. 6. (a) The impedance and phase angle of the PA load network, (b) second and third harmonic suppression levels.

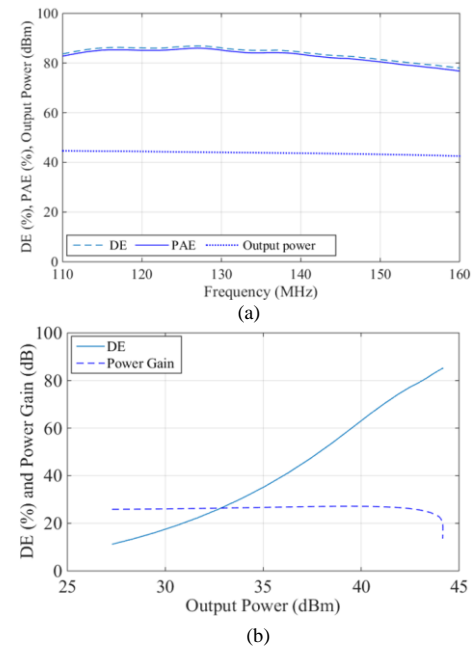


Fig. 7. Simulated (a) DE, PAE, and output power versus frequency, (b) DE and power gain versus output power at 135 MHz.

IV. MEASUREMENTS RESULTS

In order to validate the concept and analytical derivation described in Section II as well as the simulation results in Section III, we built a PA prototype on a 0.508 mm RO4003C substrate with a dielectric constant of 3.55. The photograph of the PA is shown in Fig. 8(a) with an overall board size of 68

mm \times 37 mm. The PA uses an MRFE6VS25N transistor with $V_{\text{sat}} = 2$ V as a switching device and Wurth inductors. The amplifier was driven by R&S 4320-MHz SMHU signal generator. The output power was measured using an Agilent Technologies 8563E spectrum analyzer. A 20-dB attenuator was inserted between the PA and the spectrum analyzer. The gate and drain voltages were applied using a MP3005D 30-VDC power supply. The simulated and measured input reflection coefficient (S_{11}) are shown in Fig. 8(b), with a good agreement between them being achieved. Fig. 8(c) shows the measured output power, power gain, PAE and DE at 26 dBm input power and 35 V supply voltage. Maximum output power of 41.5-44 dBm, power gain 20-22 dB, PAE of 74-80.5 % and DE of 79-82.2% are achieved over the bandwidth of interest from 115 to 155 MHz. The comparison of our work with other PAs is shown in Table II. Compared with other published works, the proposed PA has better efficiency and higher output power.

Table II: Comparison with other works.

Ref	f (MHz)	FBW (%)	Pout (W)	η / PAE (%)	2 nd /3 rd HS (dBc)	Technology
[11]	200-310	43	17.8	80/-	-	GaN FET
[12]	470-780	51	10	-70	-	LDMOS
[13]	480-730	41	10	-70	-	GaN
[14]	100-200	66	-	69/-	-	LDMOS
[15]	136-174	24	8	74/-	-	LDMOS
This Work	115-155	30	25	82.2/80.5	-30/-30	LDMOS

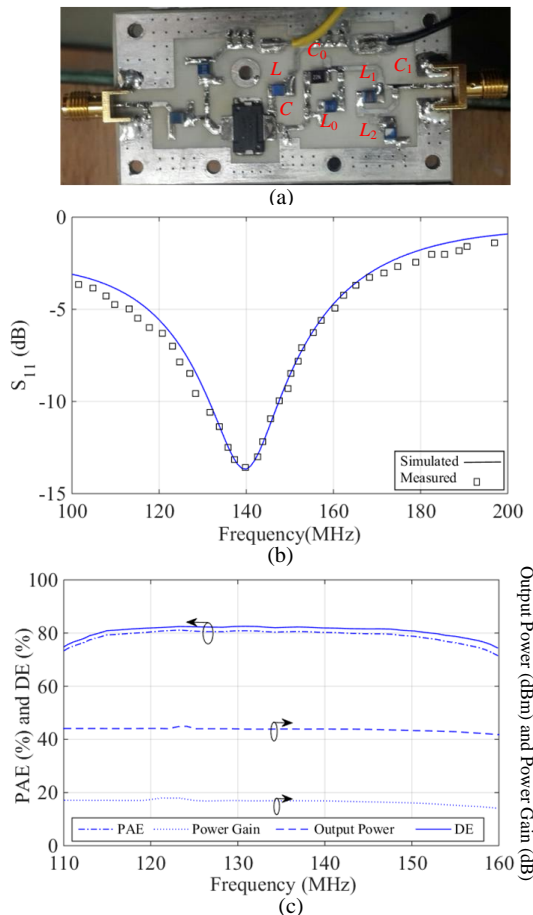


Fig. 8. (a) Photograph of the fabricated PA, (b) Simulated and measured S_{11} , (c) measured output power, power gain, PAE, and DE versus frequency.

V. CONCLUSION

A broadband parallel-circuit Class-E PA with second harmonic control circuit has been analyzed using double reactance compensation technique, and implemented using an LDMOS transistor for a robust verification. The second harmonic trap presents a low impedance to the ground to the second harmonic component whereas the series resonator L_0 - C_0 presents a high impedance to other higher harmonic components (3rd, 4th, etc.), thereby reducing the total harmonic distortion of the PA. The constructed prototype delivered a maximum DE of 82.2 % and maximum output power of 25 W.

REFERENCES

- [1] D. D. Venuto, G. Mezzina, and J. Rabaey, "Automatic 3D design for efficiency optimization of a Class E power amplifier," *IEEE Trans. Circuits Syst. II, Exp. Briefs*, vol. 65, no. 2, pp. 201-205, Feb. 2018.
- [2] A. Barakat, M. Thian, and V. Fusco, "A high-efficiency GaN Doherty power amplifier with blended Class-EF mode and load-pull technique," *IEEE Trans. Circuits Syst. II, Exp. Briefs*, vol. 65, no. 2, pp. 151-155, Feb. 2018.
- [3] P. Chen, K. Yang, and T. Zhang, "Analysis of a Class-E power amplifier with shunt filter for any duty ratio," *IEEE Trans. Circuits Syst. II, Exp. Briefs*, vol. 64, no. 8, pp. 857-861, Aug. 2017.
- [4] M. Thian and V. F. Fusco, "Analysis and design of Class-E₃F and transmission-line Class-E₃F₂ power amplifiers," *IEEE Trans. Circuits Syst. I, Reg. Papers*, vol. 58, no. 5, pp. 902-912, May 2011.
- [5] M. Thian and V. F. Fusco, "Transmission-line Class-E power amplifier with extended maximum operating frequency," *IEEE Trans. Circuits Syst. II, Exp. Briefs*, vol. 58, no. 4, pp. 195-199, Apr. 2011.
- [6] N. O. Sokal and A. D. Sokal, "Class E – A new class of high-efficiency tuned single-ended switching power amplifiers," *IEEE J. Solid-State Circuits*, vol. 10, no. 3, pp. 168-176, Jun. 1975.
- [7] F. H. Raab, "Idealized operation of the Class-E tuned power amplifier," *IEEE Trans. Circuits Syst.*, vol. 24, no. 12, pp. 725-735, Dec. 1977.
- [8] A. V. Grebennikov and H. Jaeger, "Class E with parallel circuit - A new challenge for high-efficiency RF and microwave power amplifiers," *IEEE MTT-S Int. Microw. Symp.*, 2002, pp. 1627-1630.
- [9] M. D. Wei, D. Kalim, D. Erguvan, S. F. Chang, and R. Negra, "Investigation of wideband load transformation networks for Class-E switching-mode power amplifiers," *IEEE Trans. Microw. Theory Techn.*, vol. 60, no. 6, pp. 1916-1927, Jun. 2012.
- [10] K. Shi, D. A. Calvillo-Cortes, L. C. Vreede, and F. van Rijs, "A compact 65 W 1.7-2.3 GHz Class-E GaN power amplifier for base stations," *Eur. Microw. Integr. Circuits Conf.*, 2011, pp. 542-545.
- [11] R. A. Beltran, "Broadband Class-E power amplifier designed by lumped-element network transforms and GaN FETs," *IEEE MTT-S Int. Microw. Symp.*, 2015.
- [12] J. Zhou, K. A. Morris, G. T. Watkins, and K. Yamaguchi, "Improved reactance-compensation technique for the design of wideband suboptimum Class-E power amplifiers," *IEEE Trans. Microw. Theory Techn.*, vol. 63, no. 9, pp. 2793-2801, Sep. 2015.
- [13] J. Zhou, K. Morris, G. Watkins, and K. Yamaguchi, "Wideband Class-E power amplifier covering the whole UHF broadcast band," *Eur. Microw. Integr. Circuits Conf.*, 2013, pp. 336-339.
- [14] A. Grebennikov, "Simple design equations for broadband class E power amplifiers with reactance compensation," *IEEE MTT-S Int. Microw. Symp.*, 2001, pp. 2143-2146.
- [15] K. Narendra, P. Chacko, A. V. Grebennikov, and A. Mediano, "High-efficiency broadband parallel-circuit Class E RF power amplifier with reactance-compensation technique," *IEEE Trans. Microw. Theory Techn.*, vol. 56, no. 3, pp. 604-612, Mar. 2008.
- [16] T. Suetsugu, and M. K. Kazimierzczuk, "Comparison of Class-E amplifier with nonlinear and linear shunt capacitance," *IEEE Trans. Circuits Syst. I*, vol. 50, no. 8, pp. 1089-1097, Aug. 2003.
- [17] <https://www.nxp.com/docs/en/data-sheet/MRFE6VS25N.pdf>.